A Coordinate Coverage Water Area Monitoring Scheme for Multiple Unmanned Surface Vehicles in Dynamic Environments

1st Mengwei Zhang
Institute for Ocean Engineering
Shenzhen International Graduate School
Tsinghua University
Shenzhen, China
zhangmengw@sz.tsinghua.edu.cn

2nd Zhengru Ren
Institute for Ocean Engineering
Shenzhen International Graduate School
Tsinghua University
Shenzhen, China
zhengru.ren@sz.tsinghua.edu.cn

3rd Yuqing He
State Key Laboratory of Robotics
Shenyang Institute of Automation
Chinese Academy of Sciences
Shenyang, China
heyuqing@sia.cn

4th Decai Li
State Key Laboratory of Robotics
Shenyang Institute of Automation
Chinese Academy of Sciences
Shenyang, China
lidecai@sia.cn

5th Liying Yang
State Key Laboratory of Robotics
Shenyang Institute of Automation
Chinese Academy of Sciences
Shenyang, China
yangliying@sia.cn

6th Yang An
Institute for Ocean Engineering
Shenzhen International Graduate School
Tsinghua University
Shenzhen, China
anyang@sz.tsinghua.edu.cn

2025 IEEE International Conference on Unmanned Systems (ICUS) | 979-8-3315-2672-6/25/$31.00 ©2025 IEEE | DOI: 10.1109/ICUS66297.2025.11295601

***Abstract*—Effective water area monitoring is crucial for governing and protecting aquatic environments from pollution. Utilizing multiple unmanned surface vehicles (USVs) for this task delivers significant advantages, including high safety, efficiency, and low operational costs. However, traditional coverage monitoring methods struggle to adapt to the dynamic nature of water pollution areas and the movements of the USVs themselves, as pollution spreads and changes over time based on pollutant characteristics. To address this challenge, the method described in this paper enables real-time exchange of map and state information among the USV fleet. This allows the vehicles to collaboratively share real-time data on covered and uncovered areas within the monitoring task. Based on this shared situational awareness, the method calculates the desired velocity and heading for each USV. Furthermore, it leverages the natural tendency of USVs to move apart to prevent collisions and minimize redundant coverage, thereby significantly enhancing overall coverage efficiency. Real-time path planning explicitly incorporates the kinematic constraints of the USVs to ensure feasible and practical trajectories. This paper validates the coverage capability and efficiency of this method under various simulated dynamic environmental conditions. Simulation results demonstrate its effectiveness in adapting to changing maps.**

***Index Terms*—Water area monitoring, multiple unmanned surface vehicles, coverage path planning, dynamic environment map.**

I. Introduction

Approximately seventy-one percent of the Earth's surface is covered by water, making it one of humanity's most valuable and precious resources. However, water pollution remains a global challenge, driven by unsustainable industrial practices and insufficient public policies in some regions [1]. Key pollutants include industrial waste, sewage, radioactive materials, and plastic waste [2], [3]. Growing populations and expanding industrial activities are increasing demand for freshwater from reservoirs and lagoons [4], [5], yet our understanding of water quality dynamics, particularly the spatial distribution of pollutant transport pathways and source areas remains limited. Consequently, monitoring and studying water quality are essential for safeguarding public health. These efforts measure pollutant concentrations and physical water parameters, factors directly impacting human production and daily life. The dynamic characteristics of polluted areas presents significant challenges for efficient water environment monitoring. Advances in the unmanned surface vehicle (USV) technology now enable multiple USVs deployments for high-frequency, long-term water quality monitoring in target areas [6], [7]. This promising approach effectively reduces labor costs and safety risks while significantly improving task execution efficiency, offering a powerful new method for protecting aquatic environments.

The main contributions of this paper are:

• Real-time dynamic coverage planning: enabling multiple USVs to perform real-time coverage path planning within a target monitoring area featuring dynamically changing water pollution map, based on environmental data and inter-USV status information exchange.

• Kinematic-aware distributed optimization: implementing a distributed computational framework that explicitly incorporates USV kinematic constraints to optimize coverage paths.

• Comprehensive performance validation: demonstrating the method's capabilities through diverse simulation scenar-

This work was partially supported by the Shenzhen Science and Technology Program (Grant No. WDZC20231128135104001).

979-8-3315-2672-6/25/$31.00 ©2025 IEEE

ios, quantitatively evaluating coverage percentage, completion time, and total USV path length.

The remainder of this paper is organized as follows. Section II reviews related work. Section III introduces the proposed water area monitoring scheme. Section IV presents the simulation experiments and discusses the corresponding results. Finally, concluding remarks are provided in Section V.

II. Related Works

USVs offer significant advantages for water monitoring due to their inherent security, autonomy, and programmability. They enable real-time water quality assessment and sustained synoptic observations—capturing pollutant dispersion at adequate spatial resolution before significant changes occur. USVs greatly enhance the ease, temporal resolution, and spatial scale of water sampling, a critical yet pervasive and expensive activity essential for effective water resource management. Consequently, USV technology has undergone rapid development for water monitoring missions over recent decades.

Effective water quality monitoring missions require USVs to perform coverage path planning (CPP) within the target area. Operating in vast, complex water environments demands CPP algorithms with high efficiency and robustness. There is a clear need for algorithms capable of generating high-efficiency, high-quality scanning paths for USVs. Practical deployment faces challenges such as complex coastline shapes, determining optimal coverage paths, and sequencing subregions for bathymetric surveys. To address coastal bathymetry challenges, Zhao et al. [8] presented a coverage planning scheme using the Control Point Douglas-Peucker algorithm. This leverages control points to accurately represent complex coastlines and facilitates cellular decomposition. Manjanna et al. [9] addressed adaptive coverage of unknown spatial fields using an anytime planning technique for efficient, non-uniform, data-driven point sampling. For bathymetric mapping completeness, Ma et al. [10] developed an improved BA* (IBA*) algorithm using unit decomposition and map update methods to enhance continuity and environmental modeling precision. Tang et al. [11] proposed an improved biologically inspired neural network (BINN) for environments with obstacles, incorporating a template model method and jump point search algorithm to navigate around obstacles and complete coverage. Yang et al. [12] developed a sequential algorithm for cooperative CPP of multiple USVs surveying multiple regions of interest (ROIs), handling ROI boundary generation, concave polygon decomposition, and path planning. Wu et al. [13] introduced a deep reinforcement learning-based coverage strategy for maritime search and rescue, considering varying accident probabilities. Xu et al. [14] proposed a Complete Coverage Neural Network (CCNN) algorithm simplifying the neural activity differential equation using an environmental correction term. Elmakis et al. [15] presented a hybrid multi-destination reinforcement learning approach for USV-assisted oil spill cleanup, combining conventional global path planning for multi-destination spills with reinforcement learning-based CPP to adapt to dynamic spill scenarios.

Beyond USV-specific research, coverage planning for other robotic platforms is also advancing [16] [17]. Song et al. [18] proposed an online CPP algorithm based on the ε^* algorithm using an exploratory Turing machine, demonstrating strong adaptability to unknown environments. Zhu et al. [19] enhanced BINN with their Glasius BINN algorithm for complete coverage path planning of autonomous underwater vehicles. Han et al. [20] developed a CPP obstacle avoidance algorithm for underwater gliders operating in thermocline-affected sea areas. Kan et al. [21] introduced a hierarchical, hex-decomposition-based coverage planning algorithm for unknown, obstacle-rich environments, ensuring resolution-complete coverage with tunable exploration speed and smooth, constant-velocity paths for Dubins vehicles. Sridharan et al. [22] tackled the coverage time challenge of chaotic planners by optimizing both coverage time and rate for rapid environmental coverage. Mayilvaganam et al. [23] minimized turns in polygon decomposition using a tree search model and an ant colony algorithm to generate polygon access sequences with the shortest trajectory length. Yi et al. [24] introduced a Glasius BINN with n-reconfiguration states for coverage in complex, confined environments, autonomously generating global paths adapted to the robot's width via the n-th reconfiguration state.

However, current CPP research primarily focuses on traversing and repeatedly planning paths with fixed areas. Furthermore, CPP effectiveness remains heavily dependent on static environmental factors and sensor configurations, such as coastline geometry and coverage range. Significantly, no robust methods yet adequately address the challenges posed by dynamic water areas resulting from pollution diffusion or the inherent randomness of USV positioning. Key unmet requirements include achieving complete area coverage, ensuring energy efficiency, minimizing path repetition, and guaranteeing safe navigation under these dynamic conditions.

III. Methods

A. The USV Models

To simplify the analysis, we ignore roll, pitch, and heave motions, considering only the 3-degree-of-freedom (DOF) horizontal plane motion of the USV (namely surge, sway, and yaw) [25]–[27]. The USV coordinate framework is depicted in Fig.1.

$$\dot{\boldsymbol{\eta}} = \boldsymbol{R}(\psi)\boldsymbol{v} \tag{1}$$

where $\boldsymbol{R}(\psi) = \boldsymbol{R}_{z,\psi}$, $\boldsymbol{v} = [u, v, r]^{\mathrm{T}}$, $\boldsymbol{\eta} = [x, y, \psi]^{\mathrm{T}}$.

The kinematic model for each USV performing water area monitoring is defined by its state $(\boldsymbol{p}_i, \boldsymbol{v}_i) \in \mathbb{R}^m \times \mathbb{R}^m$, where $\boldsymbol{p}_i$ and $\boldsymbol{v}_i$ represent the current position and velocity vectors, respectively, of the i-th USV in an m-dimensional space. For a group of n USVs, the system dynamics are described by the following differential equation:

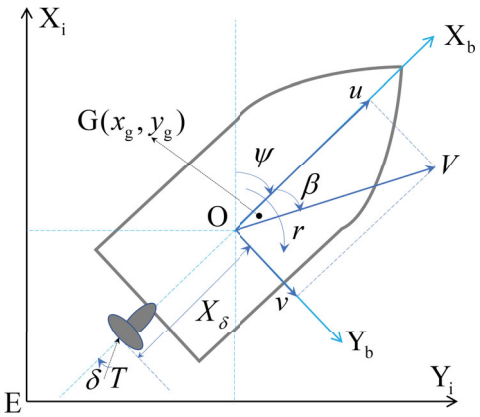

Fig. 1. The USV coordinate framework.

$$\begin{cases} \dot{\boldsymbol{p}}_i(t) = \boldsymbol{v}_i(t) \\ \dot{\boldsymbol{v}}_i(t) = \boldsymbol{u}_i(t) \end{cases} \tag{2}$$

where $\boldsymbol{v}_i = [u_i, v_i, r_i]^{\mathrm{T}}$ is the velocity of USV, $\boldsymbol{u}_i = [\dot{u}_i, \dot{v}_i, \dot{r}_i]^{\mathrm{T}}$ is the accelerated velocity of USV, $i = 1, .., n$, $n \in \mathbb{N}$, u, v, r represent the forward, lateral and turning.

During motion, water area monitoring USVs exhibit kinematic limitations such as a minimum turning radius. These constraints arise from the USV hull's rigid-body dynamics and actuator design characteristics, where both the throttle (controlling forward propulsion) and the rudder (controlling turning) exhibit saturation effects. The throttle constraint is expressed as:

$$\begin{cases} 0 \le \varepsilon_t \le \varepsilon_{\max} \\ -\Delta\varepsilon \le \varepsilon_{t+1} - \varepsilon_t \le \Delta\varepsilon \end{cases} \tag{3}$$

where ε_t represents the throttle opening at time t, $\varepsilon_{\max}$ represents the maximum throttle opening, and $\Delta\varepsilon$ represents the maximum throttle change per unit time.

Similarly, the rudder constraint is given by:

$$\begin{cases} -\delta_{\max} \le \delta_t \le \delta_{\max} \\ -\Delta\delta \le \delta_{t+1} - \delta_t \le \Delta\delta \end{cases} \tag{4}$$

where δ_t represents the rudder angle at time t, $\delta_{\max}$ represents the maximum rudder angle (where $-\delta_{\max}$ and $\delta_{\max}$ denote full left and full right rudder, respectively), and $\Delta\delta$ represents the maximum allowable rudder angle change per unit time.

When planning the desired velocity (actuated by throttle) and desired heading (actuated by rudder angle), the USV must satisfy these above constraints.

B. The Dynamic Map Information Interaction

During cooperative sailing, USVs within communication range d_c of each other are defined as neighbor vehicles. Specifically, USV i and USV j are neighbor vehicles, if:

$$N_i(t) = \{j : \|\boldsymbol{p}_j(t) - \boldsymbol{p}_i(t)\| < d_c, j = 1, 2, ..., N, j \neq i\} \tag{5}$$

where $\|\bullet\|$ denotes the Euclidean norm in $\mathbb{R}^2$. This reciprocal relationship satisfies $j \in N_i i \in N_j$where N_i is the neighbor set of USV i.

The environmental coverage map for USV i is represented as a discrete grid map $\boldsymbol{M}_i = [m_i(\boldsymbol{x})]$, where $\boldsymbol{x} = (x, y)$ denotes the center coordinates of each grid cell. Coverage status is binary:

$$m_i(\boldsymbol{x}) = \begin{cases} 1(\text{covered}) \\ 0(\text{uncovered}) \end{cases} \tag{6}$$

Given the sensor of each water area monitoring USV have a detection range of d_s, then:

$$m_i(\boldsymbol{x}) = \{\|m(\boldsymbol{x}) - \boldsymbol{p}_i(t)\| < d_s\} \tag{7}$$

Neighbor USVs $j \in N_i$ exchange coverage maps.

$$m_i(\boldsymbol{x}) = m_j(\boldsymbol{x}) \tag{8}$$

After information interaction, their maps synchronize through the union operation: $\boldsymbol{M}_i = \boldsymbol{M}_j = [m_i(\boldsymbol{x}) + m_j(\boldsymbol{x})]$.

To model dynamic pollution dispersion, the size of rectangular monitoring area (the water monitoring area could be regarded simplified as a rectangle) expands over time. The map dimensions evolve as:

$$\begin{cases} \boldsymbol{M}(t) = l_x(t) \times l_y(t) \\ \boldsymbol{M}(t+1) = l_x(t+1) \times l_y(t+1) \end{cases} \tag{9}$$

$$\begin{cases} l_x(t+1) = l_x(t) + \Delta d \\ l_y(t+1) = l_y(t) + \Delta d \end{cases} \tag{10}$$

where $l_x(t)$ and $l_y(t)$ are the length and width of the water area map at time t, Δd is the spatial expansion per unit time.

C. Water Area Coverage Monitoring Scheme

For multiple USVs water area coverage monitoring, their interaction dynamics are governed by a distance-dependent potential field function. To ensure differentiability at By $z = 0$, we adopt the following σ-norm mapping from reference literature [28]–[30]:

$$\|z\|_\sigma = \frac{1}{\varpi}\left[\sqrt{1 + \varpi\|z\|^2} - 1\right] \tag{11}$$

where the constant $\varpi > 0$ scales the norm. Moreover, the impulse function is defined as:

$$\rho_h(z) = \begin{cases} 1, z \in [0, h) \\ \frac{1}{2}\left[1 + cos(\pi\frac{z-h}{1-h})\right], z \in [h, 1) \\ 0, \text{otherwise} \end{cases} \tag{12}$$

where $h \in (0, 1)$. The equation (12) represents a smooth, stable dissipative system equation. Weighting the adjacency matrix yields:

$$a_{ij}(\boldsymbol{p}(t)) = \rho(\frac{\|\boldsymbol{p}_j(t) - \boldsymbol{p}_i(t)\|_\sigma}{r_\alpha}) \in [0, 1], j \neq i \tag{13}$$

where $r_\alpha = \|r\|_\sigma$. Note that $\left\|a_(ij)\right\| = 0$, when $\|\boldsymbol{p}_j - \boldsymbol{p}_i\| > r_\alpha$.

For the multiple USVs planning system, the differentiable dynamic equation can be simplified as:

$$\begin{cases} \dot{\boldsymbol{p}}_i(t) = \boldsymbol{v}_i(t) \\ \dot{\boldsymbol{v}}_i(t) = \boldsymbol{u}_i^{\alpha}(t) + \boldsymbol{u}_i^{\gamma}(t) \end{cases} \tag{14}$$

where $\boldsymbol{u}_i^{\alpha}(t)$ represents the control vector for the interaction between each USV, and $\boldsymbol{u}_i^{\gamma}(t)$ represents the control vector for tracking the virtual target point. Each USV obtains positions of neighbor USVs within the communication range d_c and nearest obstacles within sensor range d_s. From equation (5), neighbor USVs satisfy:

$$N_i^{\alpha}(t) = \{j : \|\boldsymbol{p}_j(t) - \boldsymbol{p}_i(t)\| < r_c, j = 1, 2, \ldots, N, j \neq i\} \tag{15}$$

In order to ensure that the inter-USV maintain a relatively safe distance d_a from each other, the $\boldsymbol{u}_i^{\alpha}(t)$ following can be calculated as:

$$\begin{aligned} \boldsymbol{u}_i^{\alpha} = & c_1^{\alpha} \sum_{j \in N_i^{\alpha}} \phi_{\alpha}\left(\|\boldsymbol{p}_j(t) - \boldsymbol{p}_i(t)\|_{\sigma}\right) \boldsymbol{n}_{ij} + \\ & c_2^{\alpha} \sum_{j \in N_i^{\alpha}} a_{ij}(\boldsymbol{p}(t))\left(\boldsymbol{v}_j(t) - \boldsymbol{v}_i(t)\right) \end{aligned} \tag{16}$$

where $\boldsymbol{n}_{ij} = \sigma_{\varpi}(\boldsymbol{p}_j(t) - \boldsymbol{p}_i(t)) = \frac{\boldsymbol{p}_j(t) - \boldsymbol{p}_i(t)}{\sqrt{1 + \varpi \|\boldsymbol{p}_j(t) - \boldsymbol{p}_i(t)\|^2}}$ represents the vector from $\boldsymbol{p}_j(t)$ to $\boldsymbol{p}_i(t)$, $\varpi \in (0, 1)$.

By tracking the virtual target points and controlling input, the $\boldsymbol{u}_i^{\gamma}(t)$ is calculated as follows:

$$\boldsymbol{u}_i^{\gamma} = -c_1^{\gamma}(\boldsymbol{p}_i(t) - \boldsymbol{p}_i^t(t)) - c_2^{\gamma}\boldsymbol{v}_i \tag{17}$$

where $\boldsymbol{p}_i^t(t) \in \mathbb{R}^m$ is the virtual target coordinate position of the i-th USV at time $t_k > 0$, and $c_{\eta}^{\nu} > 0$, $\eta = 1, 2$ and $\nu = \alpha, \gamma$ are positive constant parameter, .

According to the algorithm, the position of the virtual target point $\boldsymbol{p}_i^t(t)$ is determined by the revenue function equation. The revenue function equation is:

$$\xi_i = (1 - |m_i(\boldsymbol{x})|)(\rho_{\gamma} + (1 - \rho_{\gamma})\lambda_i(\boldsymbol{x})) \tag{18}$$

where ρ_{γ} is a constant value, and the functional equation λ_i is defined by:

$$\lambda_i(\boldsymbol{x}) = exp(-k_1 \|\boldsymbol{p}_i(t) - \boldsymbol{x}\| - k_2 \left\|\boldsymbol{p}_i^t(t) - \boldsymbol{x}\right\|) \tag{19}$$

where k_1 and k_2 are positive constant values.

The revenue value of each grid can be calculated through Equation (16). The selection of the virtual target point position at time $t_k + 1$ follows the following objective function equation:

$$\boldsymbol{p}_i^t(t_k + 1) = \underset{x \in \chi_i}{\operatorname{argmax}} \xi_i(\boldsymbol{x}, t_k) \tag{20}$$

where $\widetilde{\chi}_i = \{\boldsymbol{x} | \boldsymbol{x} \in \chi, \|\boldsymbol{x} - \boldsymbol{p}_j\| \geq \|\boldsymbol{x} - \boldsymbol{p}_j\| > r_s, j \in N_i^{\alpha}\}$, where χ is the set of all grid point centers.

According to the section II, for USVs, the communication range is d_c and the exploration coverage distance is d_s. When the USV mission begins ($t_k = 0$), all the water area maps have not been covered ($\boldsymbol{M}_i = 0$). When a water area map is covered by the USV ($\|\boldsymbol{x} - \boldsymbol{p}_i(t)\| \leq r_s$, as shown in Fig.2, pink regions).

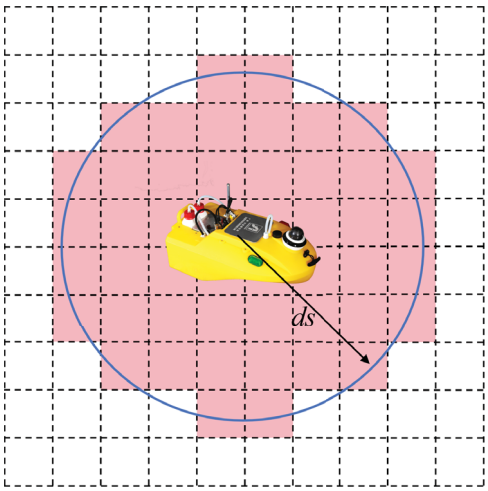

Fig. 2. The USV illustration of coverage area.

When the conditions of USVs statisfy $\|\boldsymbol{p}_j(t_k) - \boldsymbol{p}_i(t_k)\| < r_c$, they synchronize maps ($\boldsymbol{M}_i(t_k) = \boldsymbol{M}_j(t_k)$) and recompute virtual targets $\boldsymbol{p}_i^t$ to minimize coverage overlap, thereby reducing energy consumption and improving monitoring efficiency.

IV. Simulation Experiments

To evaluate the proposed method, we conducted multiple simulation experiments, with corresponding results presented in this section.

A. Simulation Design

Firstly, we designed some simulation experiments for multiple USVs coverage path planning in dynamic environment maps. Throughout all simulation experiments, we maintained consistent paramenters: the map and USV's state resolution is 0.5 m, the USV's state update frequency is 10 Hz. The communication distance between USVs is $d_c = 20$ m, the area exploration distance is $d_s = 5$ m. The USV initial velocity is uniformly randomized in $[-1, 1]^2$ m/s, the initial positions of all of USVs are randomly generated. Parameter values and weighting factors (tuned through simulation) are provided in Table. I.

TABLE I
Parameters Setting

c_1^{α}	c_2^{α}	c_1^{γ}	c_2^{γ}	k_1	k_2	ρ_{γ}
60	16	30	12	0.04	0.01	0.2

All simulation experiments were executed in MATLAB on a workstation with a 2.1 GHz Intel Core i7 processor, 32 GB RAM, Windows 11 operating system.

B. Simulation Results

The initial monitoring area measures 30×30 units, expanding to a maximum size of 50×50 units due to simulated pollution dispersion. Five USVs were deployed in the following simulation experiments. Fig.3 through Fig.5 illustrate the

coverage monitoring process at start, intermediate, and final stages.

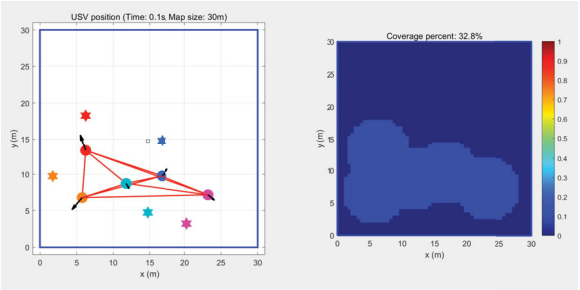

Fig. 3. The start of coverage monitoring process.

In Fig.3 - Fig.5, the left subfigure shows a screenshot of the coverage monitoring dynamic process. In this subfigure, the colored solid circles represent USVs' positions, the colored hexagonal stars represent the virtual target points, and the black arrows from solid circles represent the actual planned trajectories at that time. The right subfigure shows the display of the coverage area during the monitoring process, the color changes from light to dark, indicating the temporal sequence of coverage monitoring.

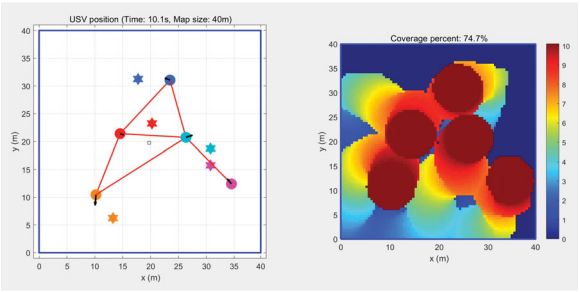

Fig. 4. The intermediate of coverage monitoring process.

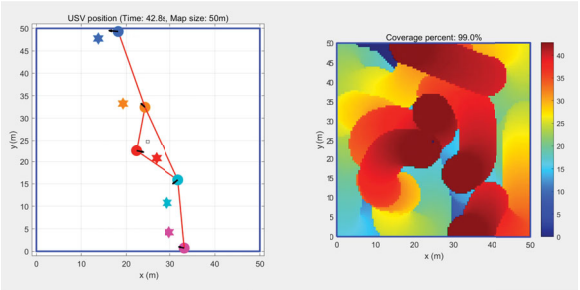

Fig. 5. The final of coverage monitoring process.

Fig.6 presents trajectory analysis. While each USV independently calculates its course and velocity based on its own coverage mission and real-time coverage status, resulting in varying path lengths, their collective behavior shows consistent operational patterns.

The whole process of coverage monitoring progression is quantified in Fig.7. The visualization tracks mission completion at (30, 45, 60, 75, 90, and 99) percent coverage

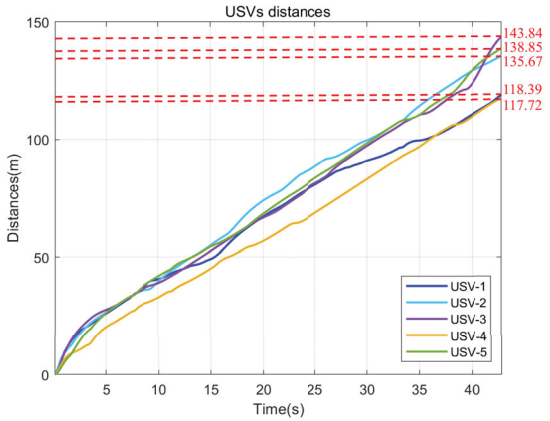

Fig. 6. The total monitoring distances of five USVs.

thresholds. The pink regions represent the area that has been covered by USVs. Early-stage coordination minimizes redundant coverage, while the 99 percent threshold signifies mission completion by all USVs.

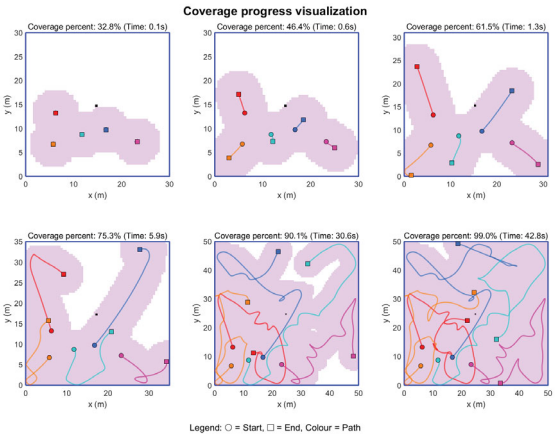

Fig. 7. Coverage monitoring status and coverage percent at different times.

Fig.8 compares coverage monitoring completion times for varying USVs fleet sizes under identical parameters. During map expansion phases, coverage times exhibit minor fluctuations. As the number of USVs increases, total area coverage monitoring time decreases significantly.

V. Conclusion

This research paper presents a novel real-time coverage method for dynamic water pollution monitoring using multiple USVs. The method addresses key challenges associated with the spatiotemporal dynamic evolution of water pollution and the USV kinematic constraints through real-time inter USVs information interaction, calculating desired velocities and headings, collision-free trajectory optimization, and minimization of redundant coverage. Comprehensive simulation experiments demonstrate the method's effectiveness and efficiency in achieving coverage within dynamic environment

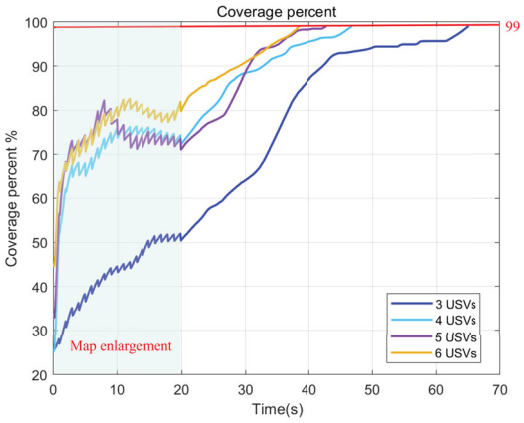

Fig. 8. Comparison of monitoring time covered by different numbers of USVs.

maps. This work represents a significant advancement toward USVs for water pollution control and broader environmental protection.

ACKNOWLEDGMENT

This work was partially supported by the Shenzhen Science and Technology Program (Grant No. WDZC20231128135104001).

REFERENCES

[1] J. R. Jambeck, R. Geyer, C. Wilcox, T. R. Siegler, M. Perryman, A. Andrady, R. Narayan, and K. L. Law, "Plastic waste inputs from land into the ocean," *science*, vol. 347, no. 6223, pp. 768–771, 2015.

[2] Z. Zhong, M. Burhan, K. C. Ng, X. Cui, and Q. Chen, "Low-temperature desalination driven by waste heat of nuclear power plants: A thermo-economic analysis," *Desalination*, vol. 576, p. 117325, 2024.

[3] Q. Chen, F. H. Akhtar, M. Burhan, K. C. Ng *et al.*, "A novel zero-liquid discharge desalination system based on the humidification-dehumidification process: a preliminary study," *Water Research*, vol. 207, p. 117794, 2021.

[4] Q. Chen, M. Burhan, M. W. Shahzad, D. Ybyraiymkul, F. H. Akhtar, Y. Li, and K. C. Ng, "A zero liquid discharge system integrating multi-effect distillation and evaporative crystallization for desalination brine treatment," *Desalination*, vol. 502, p. 114928, 2021.

[5] Q. Chen, S. Oh, Y. Li, and M. K. Ja, "Thermodynamic optimization of a low-temperature desalination system driven by sensible heat sources," *Energy*, vol. 192, p. 116633, 2020.

[6] M. Zhang, D. Li, J. Xiong, and Y. He, "Multi-dimensional water sampling unmanned surface vehicle development and application," *International journal of dynamics and control*, vol. 11, no. 6, pp. 3188–3208, 2023.

[7] M. Zhang, D. Li, Y. He, J. Xiong, Z. Li, and C. Xiong, "Autonomous water sampling system and experiment based on the unmanned surface vehicle," in *2021 IEEE International Conference on Unmanned Systems (ICUS)*. IEEE, 2021, pp. 608–613.

[8] L. Zhao, Y. Bai, and J. K. Paik, "Optimal coverage path planning for usv-assisted coastal bathymetric survey: Models, solutions, and lake trials," *Ocean Engineering*, vol. 296, p. 116921, 2024.

[9] S. Manjanna and G. Dudek, "Data-driven selective sampling for marine vehicles using multi-scale paths," in *2017 IEEE/RSJ International Conference on Intelligent Robots and Systems (IROS)*. IEEE, 2017, pp. 6111–6117.

[10] Y. Ma, Y. Zhao, Z. Li, X. Yan, H. Bi, and G. Królczyk, "A new coverage path planning algorithm for unmanned surface mapping vehicle based on a-star based searching," *Applied Ocean Research*, vol. 123, p. 103163, 2022.

[11] F. Tang, "Coverage path planning of unmanned surface vehicle based on improved biological inspired neural network," *Ocean Engineering*, vol. 278, p. 114354, 2023.

[12] S. Yang, J. Huang, X. Xiang, J. Li, and Y. Liu, "Cooperative survey of seabed rois using multiple usvs with coverage path planning," *Ocean Engineering*, vol. 268, p. 113308, 2023.

[13] J. Wu, L. Cheng, S. Chu, and Y. Song, "An autonomous coverage path planning algorithm for maritime search and rescue of persons-in-water based on deep reinforcement learning," *Ocean engineering*, vol. 291, p. 116403, 2024.

[14] P.-F. Xu, Y.-X. Ding, and J.-C. Luo, "Complete coverage path planning of an unmanned surface vehicle based on a complete coverage neural network algorithm," *Journal of Marine Science and Engineering*, vol. 9, no. 11, p. 1163, 2021.

[15] O. Elmakis and A. Degani, "Usv port oil spill cleanup using hybrid multi-destination rl-cpp," *IEEE Access*, vol. 11, pp. 122 722–122 735, 2023.

[16] M. Hassan and D. Liu, "Ppcpp: A predator–prey-based approach to adaptive coverage path planning," *IEEE Transactions on Robotics*, vol. 36, no. 1, pp. 284–301, 2019.

[17] K. R. Jensen-Nau, T. Hermans, and K. K. Leang, "Near-optimal area-coverage path planning of energy-constrained aerial robots with application in autonomous environmental monitoring," *IEEE Transactions on Automation Science and Engineering*, vol. 18, no. 3, pp. 1453–1468, 2020.

[18] J. Song and S. Gupta, "$varepsilon*$: An online coverage path planning algorithm," *IEEE Transactions on Robotics*, vol. 34, no. 2, pp. 526–533, 2018.

[19] B. Sun, D. Zhu, C. Tian, and C. Luo, "Complete coverage autonomous underwater vehicles path planning based on glasius bio-inspired neural network algorithm for discrete and centralized programming," *IEEE transactions on cognitive and developmental systems*, vol. 11, no. 1, pp. 73–84, 2018.

[20] G. Han, Z. Zhou, T. Zhang, H. Wang, L. Liu, Y. Peng, and M. Guizani, "Ant-colony-based complete-coverage path-planning algorithm for underwater gliders in ocean areas with thermoclines," *IEEE Transactions on Vehicular Technology*, vol. 69, no. 8, pp. 8959–8971, 2020.

[21] X. Kan, H. Teng, and K. Karydis, "Online exploration and coverage planning in unknown obstacle-cluttered environments," *IEEE Robotics and Automation Letters*, vol. 5, no. 4, pp. 5969–5976, 2020.

[22] K. Sridharan and Z. N. Ahmadabadi, "A multi-system chaotic path planner for fast and unpredictable online coverage of terrains," *IEEE Robotics and Automation Letters*, vol. 5, no. 4, pp. 5268–5275, 2020.

[23] K. Mayilvaganam, A. Shrivastava, and P. Rajagopal, "An optimal coverage path plan for an autonomous vehicle based on polygon decomposition and ant colony optimisation," *Ocean Engineering*, vol. 252, p. 111101, 2022.

[24] L. Yi, A. Y. S. Wan, A. V. Le, A. A. Hayat, Q. Tang, and R. E. Mohan, "Complete coverage path planning for reconfigurable omni-directional mobile robots with varying width using gbnn (n)," *Expert Systems with Applications*, vol. 228, p. 120349, 2023.

[25] R. Skjetne and Z. Ren, "A survey on modeling and control of thruster-assisted position mooring systems," *Marine Structures*, vol. 74, p. 102830, 2020.

[26] M. Zhang, D. Li, J. Xiong, and Y. He, "Gbm-ilm: Grey-box modeling based on incremental learning and mechanism for unmanned surface vehicles," *Journal of Marine Science and Engineering*, vol. 12, no. 4, p. 627, 2024.

[27] J. Gu, Y. Zhang, Y. Sui, and S. Chen, "Lagrangian study of floating debris transport around the pearl river estuary in summer," *Marine Pollution Bulletin*, vol. 211, p. 117494, 2025.

[28] N. Ganganath, C.-T. Cheng, and K. T. Chi, "Distributed antiflocking algorithms for dynamic coverage of mobile sensor networks," *IEEE transactions on industrial informatics*, vol. 12, no. 5, pp. 1795–1805, 2016.

[29] H. Zhou, Z. Ren, M. Marley, and R. Skjetne, "A guidance and maneuvering control system design with anti-collision using stream functions with vortex flows for autonomous marine vessels," *IEEE Transactions on Control Systems Technology*, vol. 30, no. 6, pp. 2630–2645, 2022.

[30] Y. Shu, Y. Zhu, F. Xu, L. Gan, P. T.-W. Lee, J. Yin, and J. Chen, "Path planning for ships assisted by the icebreaker in ice-covered waters in the northern sea route based on optimal control," *Ocean Engineering*, vol. 267, p. 113182, 2023.